VISSA-PLS-DA-Based Metabolomics Reveals a Multitargeted Mechanism of Traditional Chinese Medicine for Traumatic Brain Injury

Zian Xia[1], Wenbin Liu[2], Fei Zheng[3], Wei Huang[1], Zhihua Xing[1], Weijun Peng[4], Tao Tang[1], Jiekun Luo[1], Lunzhao Yi[2], and Yang Wang[1] (ID)

Abstract

Metabolomics is an emerging tool to uncover the complex pathogenesis of disease, as well as the multitargets of traditional Chinese medicines, with chemometric analysis being a key step. However, conventional algorithms are not suitable for directly analyzing data at all times. The variable iterative space shrinkage approach-partial least squares-discriminant analysis, a novel algorithm for data mining, was first explored to screen metabolic varieties to reveal the multitargets of Xuefu Zhuyu decoction (XFZY) against traumatic brain injury (TBI) by the 7th day. Rat plasma from Sham, Vehicle, and XFZY groups was used for gas chromatography/mass spectrometry-based metabolomics. This method showed an improved discrimination ability (area under the curve = 93.64%). Threonine, *trans*-4-hydroxyproline, and creatinine were identified as the direct metabolic targets of XFZY against TBI. Five metabolic pathways affected by XFZY in TBI rats, were enriched using Metabolic Pathway Analysis web tool (i.e., phenylalanine, tyrosine, and tryptophan biosynthesis; phenylalanine metabolism; galactose metabolism; alanine, aspartate, and glutamate metabolism; and tryptophan metabolism). In conclusion, metabolomics coupled with variable iterative space shrinkage approach-partial least squares-discriminant analysis model may be a valuable tool for identifying the holistic molecular mechanisms involved in the effects of traditional Chinese medicine, such as XFZY.

Traumatic brain injury (TBI) is known as a "silent epidemic" (Simon et al., 2017). Annually, approximately 54 to 60 million people suffer from TBI worldwide (Bazarian et al., 2018). Survivors of TBI commonly live with neurocognitive deficits and physical disability and increased risk of neurodegenerative disease in the long term (Pattinson and Gill, 2018). Unfortunately, no drug has been approved in Phase III of clinical trials for treating TBI (Stocchetti et al., 2015) because of complex pathogenesis, such as burst reactive oxygen species, increased glutamate levels, destroyed blood–brain barrier (BBB), uncontrolled neuroinflammation, and obliterated synapse (Li et al., 2018; Ma et al., 2018; Ichkova et al.,

[1]Department of Integrated Traditional Chinese and Western Medicine, Xiangya Hospital, Central South University
[2]Yunnan Food Safety Research Institute, Kunming University of Science and Technology
[3]College of Electrical and Information Engineering, Hunan University
[4]Department of Integrated Traditional Chinese & Western Medicine, The Second Xiangya Hospital, Central South University

Corresponding Authors:

Yang Wang, Department of Integrated Traditional Chinese and Western Medicine, Xiangya Hospital, Central South University, Changsha 410008, People's Republic of China.
Email: wangyang_xy87@csu.edu.cn
Lunzhao Yi, Yunnan Food Safety Research Institute, Kunming University of Science and Technology, Kunming 650500, People's Republic of China.
Email: yilunzhao@kmust.edu.cn

2019). Thus, the consensus of multitarget intervention was formed as its therapeutic principle. The multitarget property and advantageous efficacy of traditional Chinese medicine (TCM) in TBI has attracted much attention (Xing et al., 2016) and has encouraged exploration of the integrative pathogenesis of TBI and the multitargeted pharmacomechanism of TCM through various omics technologies (Tu et al., 2014; Zheng, Wang, et al., 2017; Lipponen et al., 2018).

Metabolomics is a common tool to uncover the pathogenesis of disease by reflecting the global metabolic profiling framework (Li et al., 2018). It is also employed to elucidate the molecular mechanism of TCM herbs (Xiang et al., 2011; Abdul Majid et al., 2020). It is a crucial step in high-resolution analytics, together with chemometric tools, to derive an integrated picture of endogenous and xenobiotic metabolism (Don et al., 2012). The appropriate algorithm can provide deeper insights into the integrative mechanisms of specific diseases or therapeutic interventions. The current algorithms for metabolomics analysis primarily involve principal component analysis, partial least squares-discrimination analysis (PLS-DA), orthogonal PLS-DA, support vector machines (SVM), and random forests (Gromski et al., 2015). However, these conventional algorithms are not suitable for directly analyzing data at all times, and data mining is needed.

We proposed the variable iterative space shrinkage approach (VISSA) for variable selection in a previous study (Deng et al., 2014). This approach iteratively and smoothly shrinks the variable space to obtain the best variable combination for modeling. First, the variable space is optimized in each step according to statistical information. Next, the variable space shrinks smoothly in VISSA by considering the variable combination effects and avoiding the eliminating informative variables. Finally, the results are insensitive to parameters (e.g., sampling number or the ratio of selected models) and show improved prediction ability for calibration of data in VISSA relative to other variable selection methods (Deng et al., 2014). VISSA could thus be a potential method for digging deep into metabolomics data.

Xuefu Zhuyu decoction (XFZY) is a classic TCM herbal formula in clinical practice. Recent basic and clinical evidence has demonstrated that it exerts neuroprotection against TBI (Wang, 2010; Xing et al., 2016). Its pharmacomechanisms involve synaptic regulation (Zhu et al., 2018), anti-inflammation (Xing, et al., 2016), antiapoptosis, and antioxidant effects (Zhong et al., 2018). Considering the successful application of metabolomics for uncovering TBI-related pathomechanisms (Banoei et al., 2018; Chitturi et al., 2018; Hogan et al., 2018), we employed gas chromatography/mass spectrometry (GC-MS) for metabolomics to explore the mechanism of XFZY against TBI in our previous studies (Feng et al., 2017; Zheng, Xia, et al., 2017). In these studies, the PLS-DA model was successfully used to distinguish the groups (i.e., Sham, Vehicle, or XFZY group) on the 1st or 3rd day post-TBI (Feng et al., 2017). However, the direct PLS-DA model was not capable of discriminating the XFZY treatment from the Vehicle group on the 7th day post-TBI (shown in Figure 1).

The present study aimed to explore the VISSA-PLS-DA for GC-MS-based metabolomics to screen metabolic variables on the 7th day post-TBI and then to elucidate the multitargeted pharmacomechanism of XFZY against TBI. Thereby, it may provide a new method for studying TCM.

Materials and Methods

Animals

Healthy male Sprague-Dawley (SD) rats (weight: 200 to 250 g) were supplied by the Laboratory Animal Research Center of Central South University, China. A controlled breeding room was used to house the rats with ad libitum access to normal standard chow diet and tap water. The temperature was maintained at 22°C to 25°C with 12 hr light/dark cycles and 50% ± 10% humidity. All rats adapted to these circumstances for at least 1 week. At the beginning of experiment, rats were fasted for 12 h with free access to water.

Model of TBI

The rat model of controlled cortical impact (CCI) was established using an electronic controlled pneumatic
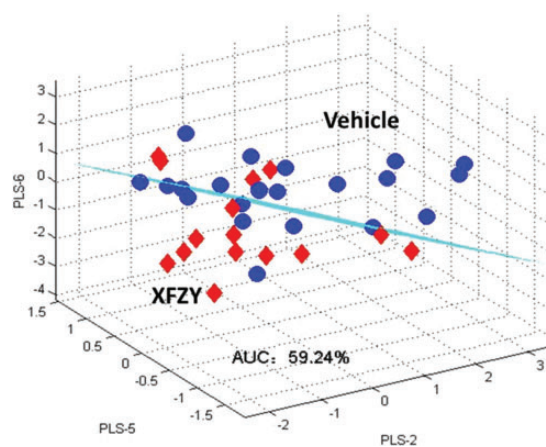
Figure 1. PLS-DA Model for Discrimination Between TBI and TBI Treated With XFZY.
Note. In total, 44 metabolic variables were directly used to establish the PLS-DA model for distinguishing the Vehicle and XFZY groups. Its AUC was 59.24%.
Vehicle = TBI rats treated with normal saline; XFZY = TBI rats treated with 9 g/kg Xuefu Zhuyu decoction; AUC = the area under receiver operating characteristic curve, evaluating the discrimination ability of classical models; PLS = partial least squares.

impact device (TBI 0310, Precision Systems & Instrumentation, Fairfax Station, VA) under 3% pentobarbital anesthesia (50 mg/kg). The parameters and procedures used were according to our previous research (Xing et al., 2016). The body temperature of rats was maintained at $37.0 \pm 0.5°C$ throughout the surgery.

Preparation of XFZY

According to the preparation method described in our previous study (Xing et al., 2016), all herbal medicines in XFZY decoction (i.e., Semen *Persicae*, Flos *Carthami*, Radix *Angelicae Sinensis*, Radix *Rehmanniae*, Radix *Achyranthis Bidentatae*, Radix *Paeoniae Rubra*, Fructus *Aurantii*, Radix *Glycyrrhizae*, Rhizoma *Chuanxiong*, Radix *Platycodonis*, and Radix *Bupleuri*) were purchased from the Pharmacy of Xiangya Hospital of Central South University (Hunan Province, PR China). The previously mentioned 11 herbs of XFZY at a ratio of 8:6:6:6:6:4:4:4:3:3:2 were decocted using purified water. The decoctions were then used to prepare a lyophilized powder of XFZY according to our previous study (Xing et al., 2016). Finally, 1 g of the freeze-dried powder contained 5.4 g of crude herbs. All powders were stored at 4°C before dissolving in distilled water for usage at a concentration of 1 g crude drugs/ml (*w/v*).

Experimental Design and Sample Collection

SD rats were randomly assigned to three groups: (a) Sham-operated group (Sham, $n = 13$): Rats underwent the same surgical procedures as CCI except no cerebral cortex trauma and gavage with an equal volume of normal saline (0.9% NaCl); (b) TBI + Vehicle (Vehicle, $n = 15$): Rats with CCI were intragastrically administered the same amount of normal saline vehicle; and (c) TBI + 9 g/kg XFZY group (XFZY, $n = 22$): Rats were orally given XFZY extract (9 g/kg body weight according to our previous study; Xing et al., 2016) after CCI. Each group was administered once per day after TBI. On the 1st, 3rd, and 7th day post-TBI, neurological function test was performed for each group. On the 7th day, all rats were sacrificed for plasma collection after the neurological function tests. The plasma samples were centrifuged at 3,000 rpm at 4°C for 10 min. The supernatants were stored at –80°C until GC-MS-based metabolomics analysis.

Assessment of Neurological Function

To assess neurological injury, the modified neurologic severity score (mNSS) was determined as in our previous study (Xing et al., 2016). The motor (muscle status and abnormal movement); sensory (visual, tactile, and proprioceptive); and reflex abilities were tested on a scale of 0 to 18 (0 normal score; 18: maximal deficit score). On the 1st, 3rd, and 7th day post-TBI, the severity of neurological injury was evaluated by mNSS.

GC-MS Data Acquisition

Sample preparation was performed according to the procedures described previously (Yi et al., 2014). Briefly, 100 μl plasma was mixed with 350 μl methanol, and 50 μl heptadecanoic acid (dissolved in methanol at a concentration of 1 mg/ml) was added as an internal standard. After vigorously vortexing for 1 min, the mixture was centrifuged at 16,000 rpm for 10 min at 4°C. The supernatant (400 μl) was transferred to a 5-ml glass centrifugation tube and evaporated to dryness under N_2 gas. Then, 70 μl of methoxyamine hydrochloride solution (20 mg/ml in pyridine) was added to the residue and incubated for 60 min at 70°C. After methoximation, 100 μl of bistrifluoroacetamide derivatization agent was added to the residue and incubated for another 50 min at 70°C. The final solution was used for GC-MS analysis. In addition, 50 μl of each original sample was pooled to generate the quality control (QC), and 100 μl aliquots of this pooled sample were pretreated through the aforementioned process. One QC sample was injected after every five sample injections to monitor the stability of the experiment (Supplementary Figure S1).

All GC-MS analyses were performed using a gas chromatography instrument (Shimadzu GC2010A, Kyoto, Japan) coupled with a mass spectrometer (GC-MS-QP2010) with a constant flow rate of helium carrier gas at 1.0 ml/min. For each sample, 1.0 μl was injected into a DB-5ms capillary column (30 m × 0.25 mm i.d., film thickness 0.25 μm). The column temperature was initially maintained at 70°C for 4 min and was then increased to 300°C at a rate of 8°C/min. Subsequently, it was held for 3 min. The total run time was 35.75 min. Mass conditions were maintained as followed: ionization voltage, 70 eV; ion source temperature, 200°C; interface temperature, 250°C; full scan mode in the 35 to 800 amu mass ranges with 0.2 s scan velocity; detector voltage, 0.9 kV.

Identification of Endogenous Metabolites and Data Processing

GC-MS data of each plasma sample, including retention characteristics, peak intensities, and integrated mass spectra, were used for the analysis. First, the automated mass-spectral deconvolution and identification system (AMDIS software, National Institute of Standards and Technology, Gaithersburg, MD, USA) was employed to support the peak finding and deconvolution. Using NIST Mass Spectral Search Program Version 2.0 (the National Institute of Standards and Technology, Gaithersburg, MD, USA) and the characteristic ions, tentative identification of the structures of peaks-of-interest was

supported by a similarity search of the NIST/EPA/NIH Mass Spectra Library (NIST05). Only metabolic features with a relative standard deviation for the relative peak areas of <30% in QC samples were retained for subsequent data analysis (Dunn et al., 2011). In all, 44 metabolites were considered as the main endogenous metabolites, and 25 metabolites were identified by their corresponding chemical standards. The biochemical databases, including the Human Metabolome Database (http://www.hmdb.ca/; Wishart et al., 2018) and the Kyoto Encyclopedia of Genes and Genomes database (Kanehisa Labs, Japan, http://www.genome.jp/kegg/), were used to search and analyze each metabolite. The peak areas of metabolites were compared with those of the internal standards to provide a semiquantitative level for the metabolites. The peak areas were extracted using our custom scripts to generate a data matrix, in which the rows represent the samples and the columns correspond to peak/area ratios to the internal standard in the same chromatogram.

Data Analysis

The data metrics of peak areas generated from metabolic profiles were analyzed by PLS-DA to establish any "groupings" with respect to the Vehicle, Sham, and XFZY group. In this study, the VISSA was employed to select the marked variables (metabolites; Deng et al., 2014; Zhang et al., 2015): The first step was to create a binary matrix $K \times P$ for sampling; the second step was to carry out weighted binary matrix sampling based on the weights of variables obtained in Step 1 and create new submodels and then to calculate the mean root mean square error of cross-validation (RMSECV) of the best new submodels; the third step was to compare the mean RMSECV$_i$ with the mean RMSECV$_{i-1}$; and the fourth step was to repeat Steps 1 to 3 using the candidate variable set and obtain a new variable set.

VISSA was calculated 500 times. The selected metabolites with high frequency (frequency ≥80% of total times) were regarded as potential biomarkers. After variable selection, PLS-DA models were established to distinguish between the Vehicle and XFZY groups (or Vehicle group vs. Sham group) on the 7th day. Then, 10-fold cross-validation was employed to select the optimal number of latent variables and to evaluate the predictive ability of the PLS-DA model. Permutation tests were employed to evaluate the reliability of the class model and were calculated 5,000 times. In a previous study, we proved that the area under receiver operating characteristic curve (AUC) was more sensitive than the correct rate to evaluate the discrimination ability of the classical models (Yi et al., 2014). In this study, AUC was employed to evaluate the discriminant ability of model.

All data were expressed as "mean ± SD." The Mann–Whitney U test was employed to analyze each metabolite. The data from mNSS were analyzed by one-way analysis of variance with a least significant difference post hoc test using the SPSS 17.0 software package. Prism Graph Pad 5.0 software was used for graphing. $p < .05$ was considered statistically significant. All programs of PLS-DA and other methods were coded in MATLAB 2010 for Windows, and all calculations were performed on an Intel Core i7 processor-based personal computer with 16G RAM.

Metabolic Pathway Analysis

The Metabolic Pathway Analysis web tool (http://www.metaboanalyst.ca/) was used for pathway analysis as described previously (Yi et al., 2016). The metabolites for discriminating between the XFZY group and Vehicle group were input for analysis. The pathway library was selected from "*Rattus norvegicus.*" The default "hypergeometric test" was chosen for pathway enrichment analysis, and "relative-betweenness centrality" algorithms were selected for pathway topological analysis. Furthermore, 0.1 was considered as the impact-value threshold of pathway topology analysis to identify the relevant pathways (Yi et al., 2016).

Results

Metabolic Profiling of Vehicle, Sham, and XFZY

GC-MS was used to determine 44 plasma metabolites (in Table 1), which were involved in the metabolic processes of carbohydrates, amino acids, lipids, energy, organic acids, and urea. The Mann–Whitney U test was employed to calculate the significant difference for each metabolite ($p < .05$ with a signed t value of 1). As shown in Table 1, six metabolites including glycine, *trans*-4-hydroxyproline, phenylalanine, palmitic acid, linoleic acid, and oleic acid were significantly altered between the Vehicle and Sham group. Except for the significant decline of phenylalanine, the previously mentioned metabolites increased markedly in the Vehicle group compared with the Sham group. However, no significant difference for each metabolite was observed between the Vehicle group and XFZY group.

Metabolic Characteristics of XFZY-Treated TBI Rats Compared With TBI Rats

Owing to no significant difference for each metabolite in the XFZY group relative to the Vehicle group, the PLS-DA algorithm was directly used to establish a discriminant model for distinguishing these. As shown in Figure 1, the AUC of this model was 59.24%, indicating the failure of modeling with poor discriminant ability.

Table 1. Metabolic Profiling of Vehicle, Sham, and Xuefu Zhuyu Decoction Groups.

| No. | Metabolites | Relative peak area | | | T vs.C | S vs.C | KEGG | HMDB |
		Sham (S) $(n=13)$	Vehicle (C) $(n=15)$	XFZY (T) $(n=22)$	(1, $p<.05$)			
1	Pyruvic acid	0.134 ± 0.026	0.129 ± 0.020	0.131 ± 0.028	0	0	C00022	HMDB00243
2	Lactic acid[a]	3.856 ± 0.993	3.840 ± 1.032	4.001 ± 1.067	0	0	C00186	HMDB00190
3	L-alanine[a]	0.547 ± 0.091	0.549 ± 0.119	0.500 ± 0.143	0	0	C00041	HMDB00161
4	Glycine[a]	0.270 ± 0.045	0.325 ± 0.060	0.301 ± 0.088	0	1	C00037	HMDB00123
5	Methylmalonic acid	0.061 ± 0.009	0.059 ± 0.011	0.060 ± 0.014	0	0	C02170	HMDB00202
6	N-acetylglycine	0.072 ± 0.008	0.078 ± 0.019	0.073 ± 0.011	0	0	C05596	HMDB00532
7	β-hydroxybutyric acid[a]	0.077 ± 0.023	0.085 ± 0.018	0.097 ± 0.040	0	0	C00989	HMDB00710
8	L-valine[a]	0.211 ± 0.032	0.199 ± 0.051	0.193 ± 0.053	0	0	C00183	HMDB00883
9	Urea	3.366 ± 0.599	3.363 ± 0.725	3.245 ± 0.696	0	0	C00086	HMDB00294
10	L-isoleucine[a]	0.274 ± 0.038	0.264 ± 0.052	0.259 ± 0.048	0	0	C00407	HMDB00172
11	L-proline[a]	0.316 ± 0.049	0.294 ± 0.073	0.264 ± 0.093	0	0	C00148	HMDB00162
12	Succinic acid	0.025 ± 0.005	0.025 ± 0.005	0.026 ± 0.005	0	0	C00042	HMDB00254
13	Glyceric acid	0.031 ± 0.012	0.030 ± 0.015	0.036 ± 0.012	0	0	C00116	HMDB00131
14	Fumaric acid	0.015 ± 0.005	0.014 ± 0.005	0.016 ± 0.005	0	0	C00122	HMDB00134
15	Serine[a]	0.313 ± 0.038	0.303 ± 0.055	0.309 ± 0.067	0	0	C00065	HMDB00187
16	Threonine[a]	0.444 ± 0.060	0.399 ± 0.065	0.435 ± 0.093	0	0	C00188	HMDB00167
17	L-malic acid[a]	0.035 ± 0.009	0.036 ± 0.007	0.038 ± 0.009	0	0	C00497	HMDB00744
18	Pyroglutamic acid[a]	0.574 ± 0.100	0.585 ± 0.082	0.595 ± 0.125	0	0	C01879	HMDB00267
19	trans-4-hydroxyproline	0.098 ± 0.014	0.114 ± 0.016	0.101 ± 0.021	0	1	C01157	HMDB00725
20	Threonic acid[a]	0.033 ± 0.017	0.033 ± 0.014	0.038 ± 0.020	0	0	–	HMDB00943
21	Creatinine[a]	0.165 ± 0.048	0.135 ± 0.039	0.115 ± 0.053	0	0	C00791	HMDB00562
22	α-ketoglutaric acid	0.013 ± 0.006	0.015 ± 0.003	0.015 ± 0.004	0	0	C00026	HMDB00208
23	Ornithine	0.069 ± 0.021	0.070 ± 0.032	0.064 ± 0.030	0	0	C00077	HMDB03374
24	Glutamic acid[a]	0.101 ± 0.031	0.087 ± 0.026	0.095 ± 0.025	0	0	C00025	HMDB00148
25	Phenylalanine[a]	0.085 ± 0.017	0.072 ± 0.013	0.075 ± 0.018	0	1	C00079	HMDB00159
26	Aspartic acid	0.041 ± 0.014	0.040 ± 0.013	0.034 ± 0.011	0	0	C00049	HMDB00191
27	Ribitol	0.064 ± 0.030	0.053 ± 0.021	0.059 ± 0.021	0	0	C00474	HMDB00508
28	Lysine	0.06 ± 0.0370	0.088 ± 0.042	0.100 ± 0.074	0	0	C00047	HMDB00182
29	Glutamine[a]	0.032 ± 0.021	0.029 ± 0.013	0.034 ± 0.016	0	0	C00064	HMDB00641
30	Citric acid[a]	0.097 ± 0.039	0.096 ± 0.028	0.093 ± 0.033	0	0	C00158	HMDB00094
31	1,5-anhydro-d-ghlcitol	0.143 ± 0.040	0.137 ± 0.031	0.127 ± 0.019	0	0	–	HMDB41561
32	D-fructose	0.053 ± 0.012	0.051 ± 0.018	0.053 ± 0.026	0	0	C00095	HMDB00660
33	Galactose	0.097 ± 0.020	0.104 ± 0.034	0.134 ± 0.050	0	0	C01582	HMDB00143
34	D-glucose[a]	9.520 ± 1.412	9.351 ± 1.977	8.867 ± 1.183	0	0	C00031	HMDB00122
35	L-tyrosine[a]	0.113 ± 0.038	0.103 ± 0.034	0.095 ± 0.035	0	0	C00082	HMDB00158
36	Palmitic acid[a]	0.419 ± 0.081	0.533 ± 0.136	0.598 ± 0.170	0	1	C00249	HMDB00220
37	Tryptophan	0.009 ± 0.004	0.012 ± 0.006	0.013 ± 0.006	0	0	C00078	HMDB00929
38	Myo-inositol	0.139 ± 0.038	0.132 ± 0.030	0.143 ± 0.035	0	0	C00137	HMDB00211
39	Heptadecanoic acid	0.011 ± 0.003	0.011 ± 0.005	0.010 ± 0.004	0	0	–	HMDB02259
40	Linoleic acid[a]	0.268 ± 0.057	0.322 ± 0.076	0.332 ± 0.126	0	1	C01595	HMDB00673
41	Oleic acid[a]	0.280 ± 0.070	0.394 ± 0.085	0.428 ± 0.114	0	1	C00712	HMDB00207
42	Stearic acid[a]	0.324 ± 0.074	0.327 ± 0.093	0.313 ± 0.117	0	0	C01530	HMDB00827
43	Arachidonic acid[a]	0.093 ± 0.028	0.101 ± 0.017	0.103 ± 0.045	0	0	C00219	HMDB01043
44	Cholesterol[a]	0.460 ± 0.140	0.524 ± 0.144	0.580 ± 0.163	0	0	C00187	HMDB00067

Note. Relative peak area of 44 metabolites is presented as the mean ± SD. KEGG = Kyoto Encyclopedia of Genes and Genomes; HMDB = Human Metabolome Database.
[a]Identified by standard substances.

To establish an ideal discriminant model, the VISSA-PLS-DA model was employed (Figure 2). First, the frequency of metabolites was calculated by VISSA for 500 times. Then, 10 metabolites were selected by

VISSA as shown in Figure 2A, namely, threonine, *trans*-4-hydroxyproline, threonic acid, creatinine, phenylalanine, aspartic acid, 1,5-anhydro-sorbitol, galactose, tryptophan, and stearic acid. Next, a PLS-DA model

for distinguishing Vehicle and XFZY group was established according to the previously mentioned 10 metabolites (Figure 2B). Its AUC was 93.64%. These results suggested super discriminant ability for distinguishing rats treated with XFZY from TBI rats. Threonine, *trans*-4-hydroxyproline, threonic acid, creatinine, phenylalanine, aspartic acid, 1,5-anhydro-sorbitol, galactose, tryptophan, and stearic acid were selected as the potential metabolites altered by XFZY in TBI.

Metabolic Characteristics of TBI Rats Compared With Sham-TBI

Analogously, the VISSA-PLS-DA model was used to discriminate the Vehicle group from the Sham group
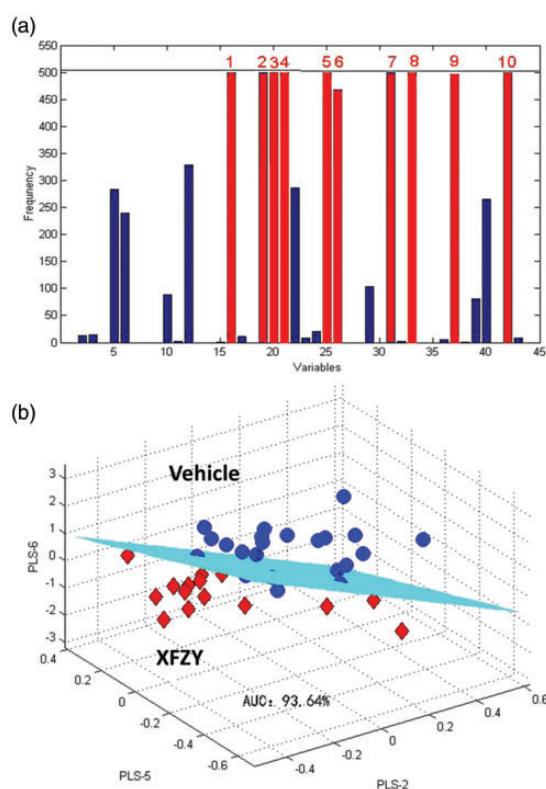
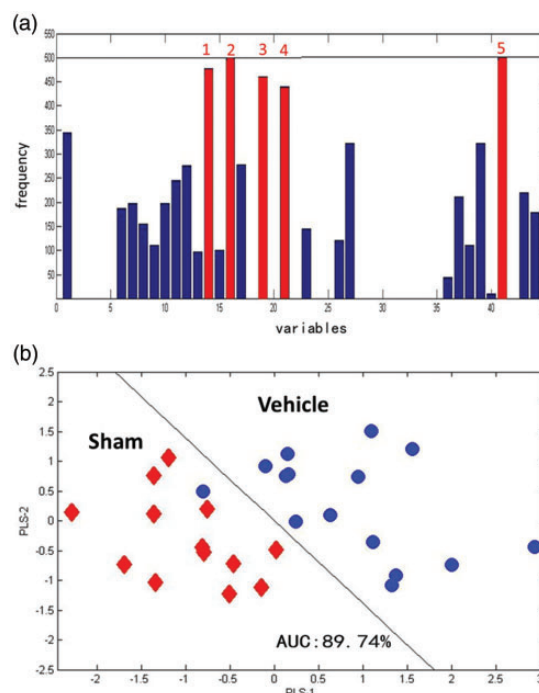**Figure 2.** VISSA-PLS-DA Model for Discrimination Between TBI and TBI Treated With XFZY.
Note. The variable iterative space shrinkage approach (VISSA) was first employed to select the marked variables from 44 metabolic variables. Then, the metabolic variables with high frequency (≥400) were used to establish the PLS-DA model for distinguishing the Vehicle and XFZY groups. (a) Frequency of each metabolite in the VISSA algorithm. The red bars are metabolites with high frequency. 1: threonine; 2: *trans*-4-hydroxyproline; 3: threonic acid; 4: creatinine; 5: phenylalanine; 6: aspartic acid; 7: 1,5-anhydro-d-ghlcitol; 8: galactose; 9: tryptophan; and 10: stearic acid. (b) PLS-DA model between the Vehicle and XFZY group. Its AUC was 93.64%.
Vehicle = TBI rats treated with normal saline; XFZY = TBI rats treated with 9 g/kg Xuefu Zhuyu decoction; AUC = the area under receiver operating characteristic curve, evaluating the discrimination ability of classical models; PLS = partial least squares.

(Figure 3). The frequency of metabolites was calculated by VISSA for 500 times, and 5 metabolites with high frequency were selected (Figure 3A), that is, threonine, *trans*-4-hydroxyproline, creatinine, fumaric acid, and oleic acid. Next, these metabolites were employed to establish a PLS-DA model (Figure 3B). The value of AUC was 89.74%, suggesting high discriminant ability. The changes in threonine, *trans*-4-hydroxyproline, creatinine, fumaric acid, and oleic acid were able to distinguish TBI rats and Sham-TBI.

## Direct Metabolic Targets of XFZY Against TBI

To elucidate the direct effective mechanism of XFZY on TBI, an intersection of two previously mentioned metabolic panels was executed. As shown in Figure 4A, threonine, *trans*-4-hydroxyproline, and creatinine were identified as the direct metabolic targets intervened by

Figure 3. VISSA-PLS-DA Model for Discrimination Between TBI and Sham-TBI.
Note. The variable iterative space shrinkage approach (VISSA) was first employed to select the marked variables from 44 metabolic variables. Then, the metabolic variables with high frequency (≥400) were used to establish the PLS-DA model for distinguishing the Vehicle and Sham groups. (a) Frequency of each metabolite in the VISSA algorithm. The red bars were metabolites with high frequency. 1: fumaric acid; 2: threonine; 3: *trans*-4-hydroxyproline; 4: creatinine; and 5: oleic acid. (b) PLS-DA model between the Vehicle and Sham group. Its AUC was 89.74%.
Vehicle = TBI rats treated with normal saline; Sham = rats without TBI treated with normal saline; AUC = the area under receiver operating characteristic curve, evaluating the discrimination ability of classical models; PLS = partial least squares.
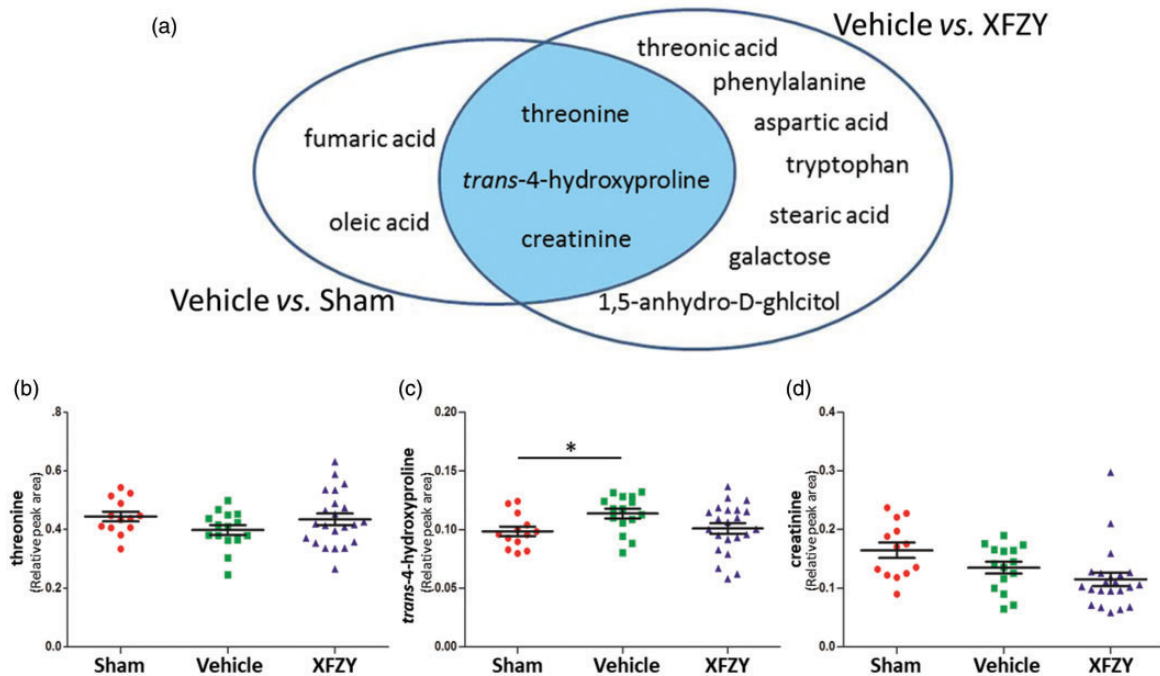
Figure 4. Effects of XFZY on Directly Modulating the Target Metabolites of TBI.

Note. (a) The intersection of two metabolic panels including threonine, *trans*-4-hydroxyproline, and creatinine was identified. The left ellipse represents the metabolic panels for discrimination between the Vehicle and Sham group. The right ellipse represents metabolic panels for discrimination between the Vehicle and XFZY group. The Scatter diagram, respectively, represents the plasma changes of threonine (b), *trans*-4-hydroxyproline (c), and creatinine (d) in the Sham, Vehicle, and XFZY groups on the 7th day post-TBI. (Data are presented as the mean $\pm$ SD, $*p < .05$ vs. the Sham group.)

Vehicle = TBI rats treated with normal saline; Sham = rats without TBI given with normal saline; XFZY = TBI rats treated with 9 g/kg Xuefu Zhuyu decoction.

XFZY. Following CCI, the levels of threonine and creatinine in plasma were decreased (Figure 4B, 4D), whereas *trans*-4-hydroxyproline was upregulated on the 7th day (Figure 4C). After treatment with 9 g/kg XFZY, the decreased threonine was recovered close to the baseline of the Sham group (Figure 4B), and the increase in *trans*-4-hydroxyproline was reversed on the 7th day (Figure 4C). Interestingly, rats treated with XFZY showed further reduced plasma levels of creatinine compared with the Vehicle group (Figure 4D).

Metabolic Pathways Intervened by XFZY in TBI

The 10 previously mentioned metabolites for discriminating between the XFZY group and Vehicle group were analyzed using Metabolic Pathway Analysis. The enriched metabolic pathways were considered as the metabolic pathways targeted by XFZY in TBI rats. As shown in Figure 5, five metabolic pathways were selected as the potential metabolic pathways regulated by XFZY. These pathways included phenylalanine, tyrosine, and tryptophan biosynthesis; phenylalanine metabolism; galactose metabolism; alanine, aspartate, and glutamate metabolism; and tryptophan metabolism.

Improvement of Neurological Function Induced by XFZY in TBI

To determine the efficacy of XFZY against TBI, the mNSS test was performed to assess the recovery of impaired neurological function on the 1st, 3rd, and 7th day post-TBI. In Figure 6, neurologic deficits were observed at predetermined timepoints from the onset of CCI, which was similar to our previous study (Xing et al., 2016). Compared with the Vehicle group, treatment with XFZY (9 g/kg) significantly contributed to the recovery of neurological deficiency, as shown by decreased mNSS scores (Figure 6). Furthermore, significant improvement of neurological functions was observed from the 3rd to 7th day post-TBI.

Discussion

The primary finding of this study is that the VISSA-PLS-DA model of GC/MS-based metabolomics is a valid method to unravel the multitargeted mechanisms of XFZY against TBI. Following this method, we found that XFZY exerted protective effects on TBI in terms of metabolic mechanisms. Threonine, *trans*-4-hydroxyproline, and creatinine were identified as the
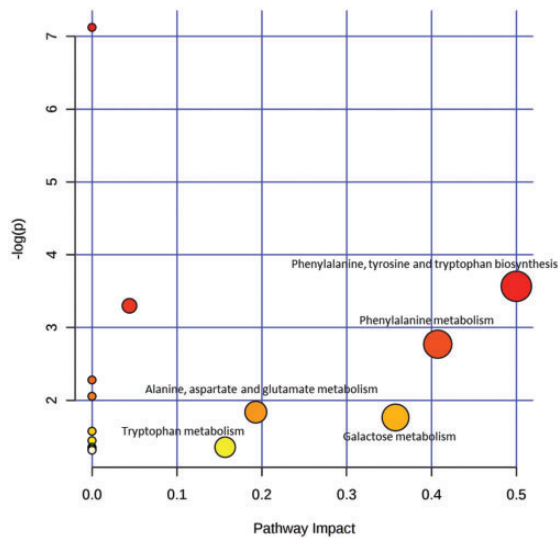
Figure 5. Summary of Enriched Metabolic Pathways Analysis Using MetPA.
Note. MetPA was used to analyze 10 screened metabolites for discriminating the Vehicle group and XFZY group, and 5 metabolic pathways of importance were enriched: (a) phenylalanine, tyrosine, and tryptophan biosynthesis; (b) phenylalanine metabolism; (c) galactose metabolism; (d) alanine, aspartate, and glutamate metabolism; and (e) tryptophan metabolism.
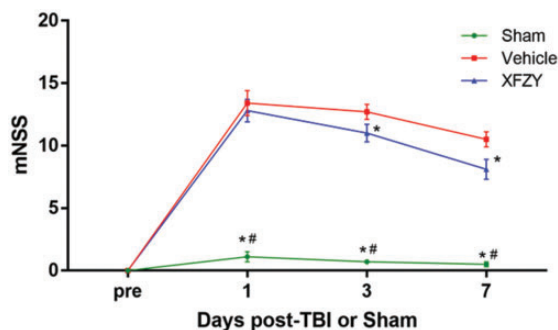
Figure 6. mNSS After TBI or Sham Injury or TBI Treated With XFZY.
Note. The mNSS test was performed to assess neurological function. Following CCI, significant increases of mNSS scores in the Vehicle group ($n = 15$) relative to the Sham group ($n = 13$) were observed from the 1st to 7th day post-TBI. Treatment with 9 g/kg XFZY ($n = 22$) significantly lowered the mNSS scores on the 3rd and 7th day compared with those in the Vehicle group. (Data are analyzed by one-way analysis of variance and presented as the mean $\pm$ SD. *$p < .05$ vs. Vehicle group; #$p < .05$ vs. XFZY group.) Vehicle = TBI rats treated with normal saline; Sham = rats without TBI treated with normal saline; XFZY = TBI rats treated with 9 g/kg Xuefu Zhuyu decoction; TBI = traumatic brain injury; mNSS = modified neurologic severity score.

direct metabolic targets of XFZY against TBI, with a concomitant rescue of impaired neurological function induced by XFZY. In addition, neuroprotection of XFZY against TBI might involve the regulation of

phenylalanine, tyrosine, and tryptophan biosynthesis; phenylalanine metabolism; galactose metabolism; alanine, aspartate, and glutamate metabolism; and tryptophan metabolism.

Our observation that alanine, aspartate, and glutamate metabolism was regulated by XFZY against TBI on the 7th day is consistent with our previous findings in metabolomics on the 1st and 3rd day post-TBI (Feng et al., 2017). These similar results support the validity of VISSA-PLS-DA to screen metabolic variables. Simultaneously, there were some differences relative to previous study (Feng et al., 2017), which may be attributed to the changes in plasma levels of metabolites with time. Intriguingly, these different metabolites including threonine, trans-4-hydroxy-L-proline, and creatinine possess its clinical significance in TBI disease.

Threonine is an essential amino acid. Its phosphorylation is one of the most prevalent posttranslational modifications that mediates diverse cellular functions (Perluigi et al., 2016). Upon onset of TBI, the activities of various serine-threonine kinases contribute to the progression of TBI pathology via phosphorylating the threonine residue of targeted proteins. For instance, the protein kinase B (Akt)/protein kinase C is related to glutamate hyperexcitability (Dorsett et al., 2016), nemo-like kinase is related to the neuronal apoptosis (Li et al., 2012), and mammalian target of rapamycin (mTOR) is involved in the neurocognitive outcome following TBI (Lu et al., 2014; Rozas et al., 2015). In our results, the changes in threonine levels in TBI rats may partly reflect the influence of the biosynthesis process of serine/threonine kinases following TBI. This effect may be further involved in the activity of serine/threonine kinases. The reverse of threonine level induced by treatment with XFZY may also refer to these processes. These speculations have been partly supported by our previous findings that the neuroprotection of XFZY against TBI involved changes in serine/threonine kinases, that is, Akt-mTOR (Xing et al., 2016).

Trans-4-hydroxy-L-proline is an important marker to assess the content of collagen in biological samples (Watanabe et al., 2015). Of these, collagen IV is one of the main components of the basal lamina, which maintains the function of the BBB (Zobel et al., 2016). Hence, the increased plasma level of *trans*-4-hydroxy-L-proline may be induced by the disruption of BBB. Treatment with XFZY attenuated this upregulation, suggesting that the neuroprotective effect of XFZY against TBI may involve functional improvement of the BBB. However, bone resorption after skull fracture also results in the release of collagens (Verissimo et al., 2015), causing an increase in *trans*-4-hydroxy-L-proline level. The decreased *trans*-4-hydroxy-L-proline induced by XFZY may also result from healing of the traumatic skull.

Further studies are needed for evidence to exclude this interference.

Creatinine is a by-product of muscle metabolism. Considering its constant generation in the living body and excretion in kidneys, its clearance (CL_{CR}) is used as an indicator for assessing renal function. Mounting evidence has shown that renal clearance of creatinine is augmented following TBI (Udy et al., 2010; Dias et al., 2015; Udy et al., 2017). This physiological link between the brain and kidney may involve a relationship between cerebrovascular autoregulation and CL_{CR}. The reasons are as follows: First, a higher CL_{CR} value in TBI was correlated with better outcome (Dias et al., 2015); furthermore, one potential mechanism from atrial natriuretic peptide (ANP) supports this relationship. The ANP is excreted through the cerebrovascular autoregulation system; it then exerts neuroprotection against edema formation and enhances CL_{CR} by elevating the permeability of glomerular capillary beds (Udy et al., 2017). The plasma level of creatinine thus reflects the ANP level to some extent. In line with these reports, we found deceased plasma level of creatinine on the 7th day post-TBI, suggesting an elevated renal clearance. After treatment with XFZY, lower levels of creatinine accompanying improved neurological function may contribute to the upregulation of ANP, which needs to be demonstrated in a further experiment.

Apart from directly targeting metabolites, the protection of XFZY against TBI may be exerted through regulating metabolic pathways. Three metabolites (phenylalanine, tryptophan, and tyrosine) were found to influence the changes in intracranial pressure and cerebral oxygen consumption ($SjvO_2$) following TBI (Vuille-Dit-Bille et al., 2012). The increased plasma phenylalanine levels were beneficial for decreasing intracranial pressure and reducing cerebral oxygen consumption (Vuille-Dit-Bille et al., 2012). In our study, treatment with XFZY increased the phenylalanine level post-TBI and contributed to the recovery of neurological function. These results indicate that the neuroprotection of XFZY may involve regulation of the three metabolic pathways relative to phenylalanine (including phenylalanine, tyrosine, and tryptophan biosynthesis; the phenylalanine metabolism; and the tryptophan metabolism). Moreover, our previous metabolomics study in TBI patients with cognitive impairment showed a disorder in galactose metabolism (Yi et al., 2016). XFZY regulated galactose metabolism in present study, which partly supports its neuroprotective role in TBI. In addition, a profound, long-lasting imbalance of alanine, aspartate, and glutamate metabolism was observed in an animal model of TBI (Amorini et al.,2017). In our study, the intervention of XFZY in this metabolic disorder may contribute to its protective mechanism. Therefore, the aforementioned evidence suggests that XFZY exerts neuroprotection against TBI through multi-intervention of metabolic pathways.

The previously mentioned clinical significance of the metabolomics results indicates that the VISSA-PLS-DA model is reasonable and scientific. Meanwhile, in terms of chemometric analysis, the VISSA-PLS-DA analytical model is more preponderant than the single PLS-DA model to discriminate two datasets. VISSA is an optimization algorithm for the selection of variable, based on weighted binary matrix sampling and model population analysis strategies (Deng et al., 2014). Its advantages include overcoming the uncertainty of a single model, generating synergistic/combination effects, and avoiding the elimination of important variables by mistake during the optimization process (Song et al., 2016). Up to now, it was mainly employed to deal with complex NIR datasets. Moreover, compared with some mainstream methods of multivariate data analysis, including iteratively retaining informative variables, competitive adaptive reweighted sampling, and Monte Carlo uninformative variable elimination, VISSA provides the lowest degree of overfitting (Talebi et al., 2015), as well as better prediction ability for the calibration of NIR data (Deng et al., 2014). Besides, novel algorithms developed from VISSA, such as iVISSA, VISSA-iPLS, and VISSA-ABC-SVM, also showed better performance for the analysis of NIR data (Deng et al., 2015; Song et al., 2016; Li et al., 2019). In our study, the VISSA algorithm improved the performance of PLS-DA model by removing the uninformative variables and interfering variables using shrinkage of variable space. In the beginning, we directly used 44 metabolites to establish the PLS-DA model for discriminating the Vehicle and XFZY groups. Its AUC was 59.24%. However, after VISSA selected 10 metabolites, the AUC value of the VISSA-PLS-DA model reached 93.64%. These results suggest the superiority of the VISSA-PLS-DA discriminative model.

However, compared with our previous research (Feng et al., 2017), there are several different results in this metabolomics study: the direct metabolic targets of XFZY against TBI, and the metabolic pathways intervened by XFZY, except for alanine, aspartate, and glutamate metabolism. These differences could originate from different points-in-time post-TBI or the number of analytical metabolites (i.e., adding seven metabolites and removing one metabolite in this study relative to our previous study). In addition, further molecular biology experiments are needed to determine whether *trans*-4-hydroxy-L-proline is involved in the recovery of BBB or in the healing of traumatic skull, as well as whether XFZY provides a neuroprotective role in TBI via upregulating the ANP levels in blood circulation. Analogously, whether the three metabolites

(threonine, *trans*-4-hydroxyproline, and creatinine) are specific targets of XFZY needs further investigation.

In summary, metabolomics based on the VISSA-PLS-DA model successfully uncovered the multitargeted mechanisms of XFZY against TBI, which are involved in modulating three direct metabolic targets (threonine, *trans*-4-hydroxyproline, and creatinine) and intervening in five metabolic pathways (phenylalanine, tyrosine, and tryptophan biosynthesis; phenylalanine metabolism; galactose metabolism; alanine, aspartate, and glutamate metabolism; and tryptophan metabolism). These findings indicate that metabolomics coupled with the VISSA-PLS-DA model is a valuable tool for identification of the holistic molecular mechanisms involved in the effects of TCM.

Ethical Approval

All animal experiments were approved by the Animal Ethics Committee of Central South University and conformed to the Guidelines for the Care and Use of Laboratory Animals (1996).

Declaration of Conflicting Interests

The author(s) declared no potential conflicts of interest with respect to the research, authorship, and/or publication of this article.

Funding

ORCID iD

Yang Wang https://orcid.org/0000-0003-0447-3107

Supplemental Material

Supplemental material for this article is available online.

References

Abdul Majid, N., Abdul Hamid, A., Salleh, S. Z., Saari, N., Abas, F., Pak Dek, M. S., Ramli, N. S., & Jaafar, A. H. (2020). Metabolomics approach to investigate the ergogenic effect of Morinda citrifolia L. leaf extract on obese Sprague Dawley rats. *Phytochem Anal*, *31*, 191–203.

Amorini, A. M., Lazzarino, G., Di Pietro, V., Signoretti, S., Lazzarino, G., Belli, A., & Tavazzi, B. (2017). Severity of experimental traumatic brain injury modulates changes in concentrations of cerebral free amino acids. *J Cell Mol Med*, *21*, 530–542.

Banoei, M. M., Casault, C., Metwaly, S. M., & Winston, B. W. (2018). Metabolomics and biomarker discovery in traumatic brain injury. *J Neurotrauma*, *35*, 1831–1848.

Bazarian, J. J., et al. (2018). Serum GFAP and UCH-L1 for prediction of absence of intracranial injuries on head CT (ALERT-TBI): A multicentre observational study. *Lancet Neurol*, *17*, 782–789.

Chitturi, J., Li, Y., Santhakumar, V., & Kannurpatti, S. S. (2018). Early behavioral and metabolomic change after mild to moderate traumatic brain injury in the developing brain. *Neurochem Int*, *120*, 75–86.

Deng, B. C., Yun, Y. H., Liang, Y. Z., & Yi, L. Z. (2014). A novel variable selection approach that iteratively optimizes variable space using weighted binary matrix sampling. *Analyst*, *139*, 4836–4845.

Deng, B. C., Yun, Y. H., Ma, P., Lin, C. C., Ren, D. B., & Liang, Y. Z. (2015). A new method for wavelength interval selection that intelligently optimizes the locations, widths and combinations of the intervals. *Analyst*, *140*, 1876–1885.

Dias, C., Gaio, A. R., Monteiro, E., Barbosa, S., Cerejo, A., Donnelly, J., Felgueiras, O., Smielewski, P., Paiva, J. A., & Czosnyka, M. (2015). Kidney-brain link in traumatic brain injury patients? A preliminary report. *Neurocrit Care*, *22*, 192–201.

Don, A. S., Tsang, C. K., Kazdoba, T. M., D'Arcangelo, G., Young, W., & Zheng, X. F. (2012). Targeting mTOR as a novel therapeutic strategy for traumatic CNS injuries. *Drug Discov Today*, *17*, 861–868.

Dorsett, C. R., McGuire, J. L., Niedzielko, T. L., DePasquale, E. A., Meller, J., Floyd, C. L., & McCullumsmith, R. E. (2016). TBI induces alterations in cortical glutamate uptake without a reduction in GLT-1 protein expression. *J Neurotrauma*, *34*, 220–234.

Dunn, W. B., Broadhurst, D., Begley, P., Zelena, E., Francis-McIntyre, S., Anderson, N., Brown, M., Knowles, J. D., Halsall, A., Haselden, J. N., Nicholls, A. W., Wilson, I. D., Kell, D. B., & Goodacre, R. (2011). Procedures for large-scale metabolic profiling of serum and plasma using gas chromatography and liquid chromatography coupled to mass spectrometry. *Nat Protoc*, *6*, 1060–1083.

Feng, D., Xia, Z., Zhou, J., Lu, H., Zhang, C., Fan, R., Xiong, X., Cui, H., Gan, P., Huang, W., Peng, W., He, F., Wang, Z., Wang, Y., & Tang, T. (2017). Metabolomics reveals the effect of Xuefu Zhuyu decoction on plasma metabolism in rats with acute traumatic brain injury. *Oncotarget*, *8*, 94692–94710.

Gromski, P. S., Muhamadali, H., Ellis, D. I., Xu, Y., Correa, E., Turner, M. L., & Goodacre, R. (2015). A tutorial review: Metabolomics and partial least squares-discriminant analysis–a marriage of convenience or a shotgun wedding. *Anal Chim Acta*, *879*, 10–23.

Hogan, S. R., Phan, J. H., Alvarado-Velez, M., Wang, M. D., Bellamkonda, R. V., Fernandez, F. M., & LaPlaca, M. C. (2018). Discovery of lipidome alterations following traumatic brain injury via high-resolution metabolomics. *J Proteome Res*, *17*, 2131–2143.

Ichkova, A., Fukuda, A. M., Nishiyama, N., Paris, G., Obenaus, A., & Badaut, J. (2019). Small interference RNA targeting connexin-43 improves motor function and limits

astrogliosis after juvenile traumatic brain injury. *ASN Neuro*, 11, 1759091419847090.

Li, Q., Wei, S., Wu, D., Wen, C., & Zhou, J. (2018). Urinary metabolomics study of patients with gout using gas chromatography-mass spectrometry. *Biomed Res Int*, 2018, 3461572.

Li, Y., Sun, J., Wu, X., Lu, B., Wu, M., & Dai, C. (2019). Grade identification of tieguanyin tea using fluorescence hyperspectra and different statistical algorithms. *J Food Sci*, 84, 2234–2241.

Li, Z., Cui, G., Wang, J., Yu, Z., Zhao, L., & Lv, Z. (2012). Nemo-like kinase (NLK) involves in neuronal apoptosis after traumatic brain injury. *Cell Mol Neurobiol*, 32, 381–389.

Li, Z., Zeng, G., Zheng, X., Wang, W., Ling, Y., Tang, H., & Zhang, J. (2018). Neuroprotective effect of formononetin against TBI in rats via suppressing inflammatory reaction in cortical neurons. *Biomed Pharmacother*, 106, 349–354.

Lipponen, A., El-Osta, A., Kaspi, A., Ziemann, M., Khurana, I., Kn, H., Navarro-Ferrandis, V., Puhakka, N., Paananen, J., & Pitkanen, A. (2018). Transcription factors Tp73, Cebpd, Pax6, and Spi1 rather than DNA methylation regulate chronic transcriptomics changes after experimental traumatic brain injury. *Acta Neuropathol Commun*, 6, 17.

Lu, Q., Gao, L., Huang, L., Ruan, L., Yang, J., Huang, W., Li, Z., Zhang, Y., Jin, K., & Zhuge, Q. (2014). Inhibition of mammalian target of rapamycin improves neurobehavioral deficit and modulates immune response after intracerebral hemorrhage in rat. *J Neuroinflamm*, 11, 44.

Ma, M. W., Wang, J., Dhandapani, K. M., Wang, R., & Brann, D. W. (2018). NADPH oxidases in traumatic brain injury – Promising therapeutic targets? *Redox Biol*, 16, 285–293.

Pattinson, C. L., & Gill, J. M. (2018). Risk of dementia after TBI – A cause of growing concern. *Nat Rev Neurol*, 14, 511–512.

Perluigi, M., Barone, E., Di Domenico, F., & Butterfield, D. A. (2016). Aberrant protein phosphorylation in Alzheimer disease brain disturbs pro-survival and cell death pathways. *Biochim Biophys Acta*, 1862, 1871–1882.

Rozas, N. S., Redell, J. B., Hill, J. L., McKenna, J., III, Moore, A. N., Gambello, M. J., & Dash, P. K. (2015). Genetic activation of mTORC1 signaling worsens neurocognitive outcome after traumatic brain injury. *J Neurotrauma*, 32, 149–158.

Simon, D. W., McGeachy, M. J., Bayir, H., Clark, R. S., Loane, D. J., & Kochanek, P. M. (2017). The far-reaching scope of neuroinflammation after traumatic brain injury. *Nat Rev Neurol*, 13, 171–191.

Song, X., Huang, Y., Yan, H., Xiong, Y., & Min, S. (2016). A novel algorithm for spectral interval combination optimization. *Anal Chim Acta*, 948, 19–29.

Stocchetti, N., et al. (2015). Neuroprotection in acute brain injury: An up-to-date review. *Crit Care*, 19, 186.

Talebi, M., Schuster, G., Shellie, R. A., Szucs, R., & Haddad, P. R. (2015). Performance comparison of partial least squares-related variable selection methods for quantitative structure retention relationships modelling of retention times in reversed-phase liquid chromatography. *J Chromatogr A*, 1424, 69–76.

Tu, T., Zhou, S., Liu, Z., Li, X., & Liu, Q. (2014). Quantitative proteomics of changes in energy metabolism-related proteins in atrial tissue from valvular disease patients with permanent atrial fibrillation. *Circ J*, 78, 993–1001.

Udy, A., Boots, R., Senthuran, S., Stuart, J., Deans, R., Lassig-Smith, M., & Lipman, J. (2010). Augmented creatinine clearance in traumatic brain injury. *Anesth Analg*, 111, 1505–1510.

Udy, A. A., Jarrett, P., Lassig-Smith, M., Stuart, J., Starr, T., Dunlop, R., Deans, R., Roberts, J. A., Senthuran, S., Boots, R., Bisht, K., Bulmer, A. C., & Lipman, J. (2017). Augmented renal clearance in traumatic brain injury: A single-center observational study of atrial natriuretic peptide, cardiac output, and creatinine clearance. *J Neurotrauma*, 34, 137–144.

Verissimo, D. M., Leitao, R. F., Figueiro, S. D., Goes, J. C., Lima, V., Silveira, C. O., & Brito, G. A. (2015). Guided bone regeneration produced by new mineralized and reticulated collagen membranes in critical-sized rat calvarial defects. *Exp Biol Med*, 240, 175–184.

Vuille-Dit-Bille, R. N., Ha-Huy, R., & Stover, J. F. (2012). Changes in plasma phenylalanine, isoleucine, leucine, and valine are associated with significant changes in intracranial pressure and jugular venous oxygen saturation in patients with severe traumatic brain injury. *Amino Acids*, 43, 1287–1296.

Wang, Z. W. (2010). 108 Cases of clinical observation of Xuefu Zhuyu on patients with post-craniocerebral traumatic syndrome. *Shanxi Zhong Yi*, 31, 850–850 [in Chinese].

Watanabe, S., Hiraoka, Y., Endo, S., Tanimoto, Y., Tozawa, Y., & Watanabe, Y. (2015). An enzymatic method to estimate the content of L-hydroxyproline. *J Biotechnol*, 199, 9–16.

Wishart, D. S., et al. (2018). HMDB 4.0: The human metabolome database for 2018. *Nucleic Acids Res*, 46, D608–D617.

Xiang, Z., Wang, X. Q., Cai, X. J., & Zeng, S. (2011). Metabolomics study on quality control and discrimination of three curcuma species based on gas chromatograph-mass spectrometry. *Phytochem Anal*, 22, 411–418.

Xing, Z., Xia, Z., Peng, W., Li, J., Zhang, C., Fu, C., Tang, T., Luo, J., Zou, Y., Fan, R., Liu, W., Xiong, X., Huang, W., Sheng, C., Gan, P., & Wang, Y. (2016). Xuefu Zhuyu decoction, a traditional Chinese medicine, provides neuroprotection in a rat model of traumatic brain injury via an anti-inflammatory pathway. *Sci Rep*, 6, 20040.

Yi, L., Dong, N., Shi, S., Deng, B., Yun, Y., Yi, Z., & Zhang, Y. (2014). Metabolomic identification of novel biomarkers of nasopharyngeal carcinoma. *RSC Adv*, 4, 59094–59101.

Yi, L., Shi, S., Wang, Y., Huang, W., Xia, Z. A., Xing, Z., Peng, W., & Wang, Z. (2016). Serum metabolic profiling reveals altered metabolic pathways in patients with post-traumatic cognitive impairments. *Sci Rep*, 6, 21320.

Zhang, X., Yi, L., Deng, B., Chen, L., Shi, S., Zhuang, Y., & Zhang, Y. (2015). Discrimination of Acori Tatarinowii Rhizoma and Acori Calami Rhizoma based on quantitative gas chromatographic fingerprints and chemometric methods. *J Sep Sci*, 38, 4078–4085.

Zheng, F., Xia, Z. A., Zeng, Y. F., Luo, J. K., Sun, P., Cui, H. J., Wang, Y., Tang, T., & Zhou, Y. T. (2017). Plasma

metabolomics profiles in rats with acute traumatic brain injury. *PLoS One*, *12*, e0182025.

Zheng, P., Wang, Y., Lu, H., Zhou, X., Tang, T., Fan, R., Zhang, C., Cui, H., Wang, Y., & Luo, J. (2017). Plasma metabolomics analysis based on GC-MS in infertile males with kidney-yang deficiency syndrome. *Evid Based Complementary Altern Med*, *2017*, Article 6270195.

Zhong, Y., Luo, J., Tang, T., Li, P., Liu, T., Cui, H., Wang, Y., & Huang, Z. (2018). Exploring Pharmacological mechanisms of Xuefu Zhuyu decoction in the treatment of traumatic brain injury via a network pharmacology approach.

Evid Based Complementary Altern Med, *2018*, Article 8916938.

Zhu, L., Tang, T., Fan, R., Luo, J. K., Cui, H. J., Zhang, C. H., Peng, W. J., Sun, P., Xiong, X. G., & Wang, Y. (2018). Xuefu Zhuyu decoction improves neurological dysfunction by increasing synapsin expression after traumatic brain injury. *Neural Regen Res*, *13*, 1417–1424.

Zobel, K., Hansen, U., & Galla, H. J. (2016). Blood-brain barrier properties in vitro depend on composition and assembly of endogenous extracellular matrices. *Cell Tissue Res*, *365*, 233–245.